minerals

MDPI

Article

Timing and Petrogenesis of Early Devonian Intrusive Rocks in the Niukutoudong Area: New Constraints on Tectonic Evolution of the East Kunlun Orogen

Yang Jin [1,2], Xiaoliang Li [2,*], Xingyu Xiao [3,*], Shoulin Cao [1,2], Wanhui Zhang [1,2], De Yang [1,2], Jun Yang [1,2], Shangwen Ji [2,4] and Ye Qian [2,3]

1 No.1 Geological Exploration Institute, Qinghai Provincial Nonferrous Metal Geological and Minerals Exploration Bureau, Xining 810007, China; jinyang202606@163.com (Y.J.)
2 Qinghai Provincial Key Laboratory of Buried Ore Exploration, Qinghai Provincial Nonferrous Metal Geological and Minerals Exploration Bureau, Xining 810007, China
3 College of Earth Sciences, Jilin University, Changchun 130061, China
4 No.2 Geological Exploration Institute, Qinghai Provincial Nonferrous Metal Geological and Minerals Exploration Bureau, Xining 810007, China
* Correspondence: lxiaoliang2026@163.com (X.L.); xiaoxy24@mails.jlu.edu.cn (X.X.)

Abstract

The Niukutoudong deposit, in the Qimantage metallogenic belt, western East Kunlun Orogenic Belt, is a recently discovered cobalt-rich polymetallic deposit. This study integrates zircon U-Pb geochronology and whole-rock geochemistry of the ore-hosting intrusions to constrain their emplacement ages, petrogenesis, and tectonic setting, thereby constraining the Early Devonian tectonic evolution of the East Kunlun area. The geochronological results for four samples demonstrate that the granite porphyry, granite, granodiorite, and gabbroic diorite at Niukutoudong were emplaced in the Early Devonian (403.7–406.3 Ma). Geochemically, the granite, granodiorite, and gabbroic diorite are high-K calc-alkaline, metaluminous to weakly peraluminous I-type granitoids, characterized by consistent enrichment in LREEs, negative Eu anomalies, enrichment in LILEs, and depletion in HFSEs. The granite porphyry, by contrast, is a peraluminous A-type granite distinguished by elevated total REE contents, pronounced negative Eu anomalies, and high HFSE abundances. The regional source characteristics of coeval intrusions, integrated with key incompatible element ratios (e.g., Nb/Ta, Ba/Nb), imply that the Early Devonian Niukutoudong intrusions were probably generated through crust–mantle interaction. Integrated evidence indicates that the Niukutoudong intrusive rocks formed in a post-collisional extensional environment following the closure of the Proto-Tethys Ocean. The mixed crust–mantle signature common to both regional and local Early Devonian intrusive rocks indicates that the East Kunlun Orogenic Belt had already transitioned from syn-collisional crustal thickening into a post-collisional extensional stage by the Early Devonian, marked by lithospheric thinning, asthenospheric upwelling, and crust–mantle interaction. This magmatism records the tectonic regime shift and likely has a genetic link with the Niukutoudong Co-polymetallic mineralization, offering critical insights into the Qimantage metallogenic framework.

Keywords: East Kunlun Orogenic Belt; Early Devonian; I-type or A-type granite; crust-mantle mixing; post-collisional extensional setting; zircon U-Pb dating; geochemistry; Qimantage

Check for updates

Academic Editors: Takeshi Hasegawa, Indranova Suhendro and Kazuya Shimooka

Received: 16 June 2026
Revised: 17 July 2026
Accepted: 23 July 2026
Published: 24 July 2026

Copyright: © 2026 by the authors. Licensee MDPI, Basel, Switzerland. This article is an open access article distributed under the terms and conditions of the Creative Commons Attribution (CC BY) license.

1. Introduction

The East Kunlun Orogenic Belt, located in the northern Tibetan Plateau, constitutes a major component of the Chinese Central Orogenic Belt (Figure 1a). Characterized by multi-period tectono-magmatic activity, this belt has undergone multiple orogenic cycles and preserves a rich record of the intricate evolutionary histories of the Proto-Tethys and Paleo-Tethys oceans [1–6]. The Early Paleozoic orogeny, in particular, is genetically tied to the tectonic evolution of the Proto-Tethys Ocean [1]. The opening and expansion of the Proto-Tethys Ocean began in the Early Cambrian [7]. This ocean began to subduct southward at ca. 520 Ma [8,9]. Subduction eventually ceased at 444.5 Ma, marking the transition to a syn-collisional stage [1]. However, the precise timing of the shift from syn-collisional convergence to post-collisional extension remains uncertain, and the deep geodynamic processes and magmatic responses associated with this pivotal transition are still debated. Resolving this tectonic regime shift is essential for deciphering post-collisional extension, lithospheric thinning, and associated mineralization.

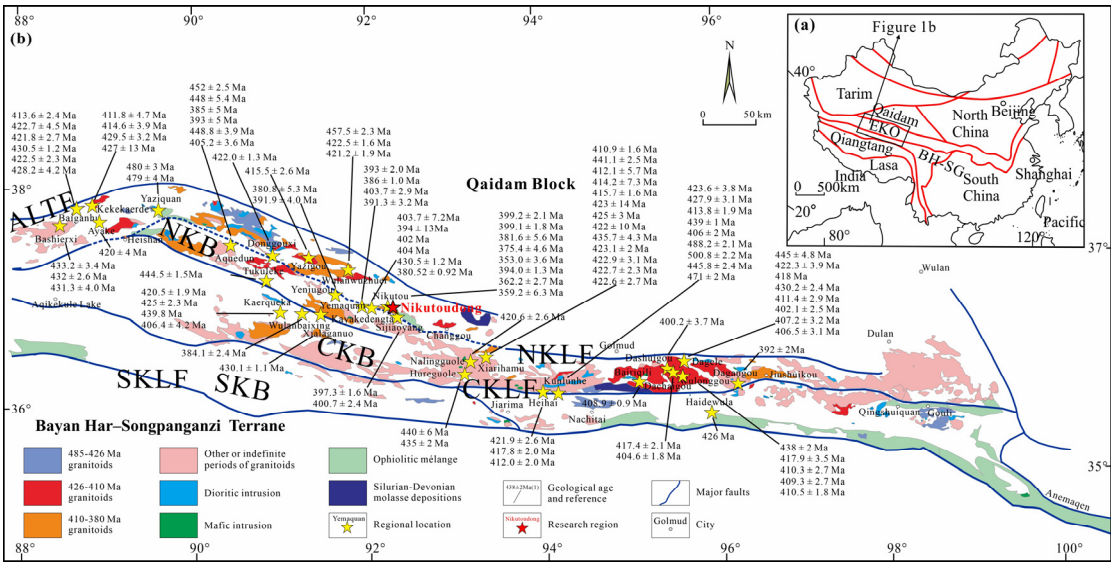


Figure 1. (**a**) The location of the East Kunlun Orogenic Belt within the tectonic framework of China (Modified from [10]); (**b**) Simplified tectonic maps of the East Kunlun Orogenic Belt (Modified from [10]). NKB: North Kunlun Belt; CKB: Central Kunlun Belt; SKB: South Kunlun Belt; ALKF: North Kunlun Fault; CKLF: Middle Kunlun Fault; SKLF: South Kunlun–Anyemaqen Fault. Age data in the figure are from [1,11–54] and references therein.

The Niukutoudong cobalt polymetallic deposit is a significant recent discovery in the Qimantage metallogenic belt of the East Kunlun Orogenic Belt. It shows a close spatial association with a suite of intermediate–felsic intrusive rocks. Previous studies have mainly focused on the regional geological setting and deposit geology [55]. However, the emplacement ages, petrogenesis, and tectonic setting of the ore-hosting intrusive rocks remain poorly constrained. These intrusive rocks provide a direct recorder of the pre-mineralization magmatic architecture and its tectonic drivers.

To address these questions, this study targets the granite porphyry, granite, granodiorite, and gabbroic diorite in the Niukutoudong area, employing systematic zircon U-Pb geochronology and whole-rock geochemical analyses. The objectives are to: (1) precisely determine the rock-forming ages of these intrusive rocks; (2) elucidate their petrogenetic type, magma source, and evolutionary processes; and (3) constrain their tectonic setting, thereby furnishing new geochronological and geochemical constraints on the Early Devonian post-collisional evolution of the East Kunlun Orogenic Belt. This work not only refines

the Early Paleozoic tectono-magmatic evolution framework of the East Kunlun area but also provides critical insights into the magmatic-controlled metallogenic background of this enriched metallogenic belt.

2. Geological Setting

The East Kunlun Orogenic Belt is located in the northern Tibetan Plateau, bordered to the north by the Qaidam Block and to the south by Bayan Har–Songpanganzi Terrane ([11]; Figure 1a,b). Delineated by the roughly EW-trending North Kunlun, Central Kunlun, and South Kunlun regional faults, the belt is subdivided into three principal tectono-magmatic units: the North Kunlun Belt, the Central Kunlun Belt, and the South Kunlun Belt ([56]; Figure 1b). The East Kunlun Orogenic Belt represents a giant magmatic belt within the Tibetan Plateau, rivaling the Gangdese Belt in scale [1]. It records a protracted succession of Proterozoic to Mesozoic tectono-thermal events, of which the Early Paleozoic (Proto-Tethys) and Late Paleozoic–Early Mesozoic (Paleo-Tethys) orogenies are the most prominent [57].

The Qimantage region, central to this study, is located in the western segment of the East Kunlun Orogenic Belt, south of the North Kunlun Belt (Figure 1b). It represents one of the most intensely active Early Paleozoic magmatic domains in the East Kunlun area, characterized by widespread exposure of Early Paleozoic granitoids [1]. The spatiotemporal distribution and geochemical signatures of these magmatic rocks provide critical tracers for reconstructing the subduction, collision, and post-collisional extension of the Proto-Tethys Ocean [58–61]. Regionally, magmatic rocks broadly coeval with the Niukutoudong intrusive rocks (~430–400 Ma) have been widely reported [16,17,20,22], comprising I-, S-, and A-type granites. These occurrences suggest that the Late Silurian to Early Devonian marked a critical juncture of tectonic regime shift and complex, multi-component magma sources.

The Niukutoudong cobalt polymetallic deposit is situated on the northern slopes of the Qimantage Mountains, southwest of the Qaidam Basin (Figures 1b and 2). The area preserves a relatively intact stratigraphic succession, comprising shallow-marine carbonate rocks and volcanic rocks of the Ordovician Qimantage Group (OQ), Carboniferous clastic–carbonate sequences (C_1dg, C_2d), and clastic rocks of the Lower–Middle Permian Dachaigou Formation ($P_{1-2}d$). These strata are overall covered by Quaternary (Q) unconsolidated sediments (Figure 2).

The regional structural grain trends predominantly NWW–SEE, conforming to the tectonic strike of the East Kunlun Orogenic Belt. Faults are pervasively developed, dominated by NWW-trending compressive-transpressional master faults, accompanied by NNE-trending transtensional secondary faults (Figure 2).

Magmatic rocks are the primary focus of this study and represent the defining geological feature of the ore district. Magmatic activity in the area is intense, and plutons are widely distributed (Figure 2). The main rock types include Devonian intermediate–felsic intrusive rocks, Ordovician volcanic rocks, and a diverse suite of acidic to intermediate–mafic dikes. Among them, the Devonian intrusive rocks are the core subject of this study, dominated by granite porphyry, granite, granodiorite, and gabbroic diorite. These intrusive rocks typically occur as stocks and are spatially intimately linked to mineralization.

All fresh samples in this study were collected from the Devonian intermediate–felsic intrusive rocks directly associated with ore formation. Petrographically, the granite porphyry is yellowish-white and has a massive structure, with a porphyritic texture defined by phenocrysts of alkali feldspar and quartz set in a microcrystalline groundmass. It consists predominantly of alkali feldspar (20%–25%), quartz (15%–20%), calcite (10%–15%), biotite (5%), and minor accessory minerals (sphene and epidote). Alkali feldspar locally displays argillic alteration (Figure 3a–c). The granodiorite is yellowish-gray, exhibits a

medium- to fine-grained subhedral granular texture and massive structure. It is composed mainly of plagioclase (35%–40%), quartz (30%–35%), biotite (5%–10%), alkali feldspar (5%), and hornblende (5%), together with accessory minerals. Plagioclase shows zoning texture and partially exhibits sericitization (Figure 3d–f). The granite is grayish-white, with a fine-grained subhedral granular texture and massive structure. It is mineralogically dominated by quartz (35%–40%), plagioclase (35%–40%), alkali feldspar (10%–15%), and biotite (5%). Plagioclase shows zoning texture. Sericitic and argillic alteration are locally developed in plagioclase and alkali feldspar. (Figure 3g–i). The gabbroic diorite is grayish-black, displaying a fine-grained subhedral granular texture and massive structure. Its major mineral assemblage comprises plagioclase (40%–45%), pyroxene (15%–20%), quartz (10%–15%), hornblende (5%), biotite (<5%), and minor accessory minerals (apatite). Plagioclase shows zoning texture and partially displays sericitization (Figure 3j–l). These petrographic characteristics provide a crucial petrological foundation for the ensuing geochemical investigations.

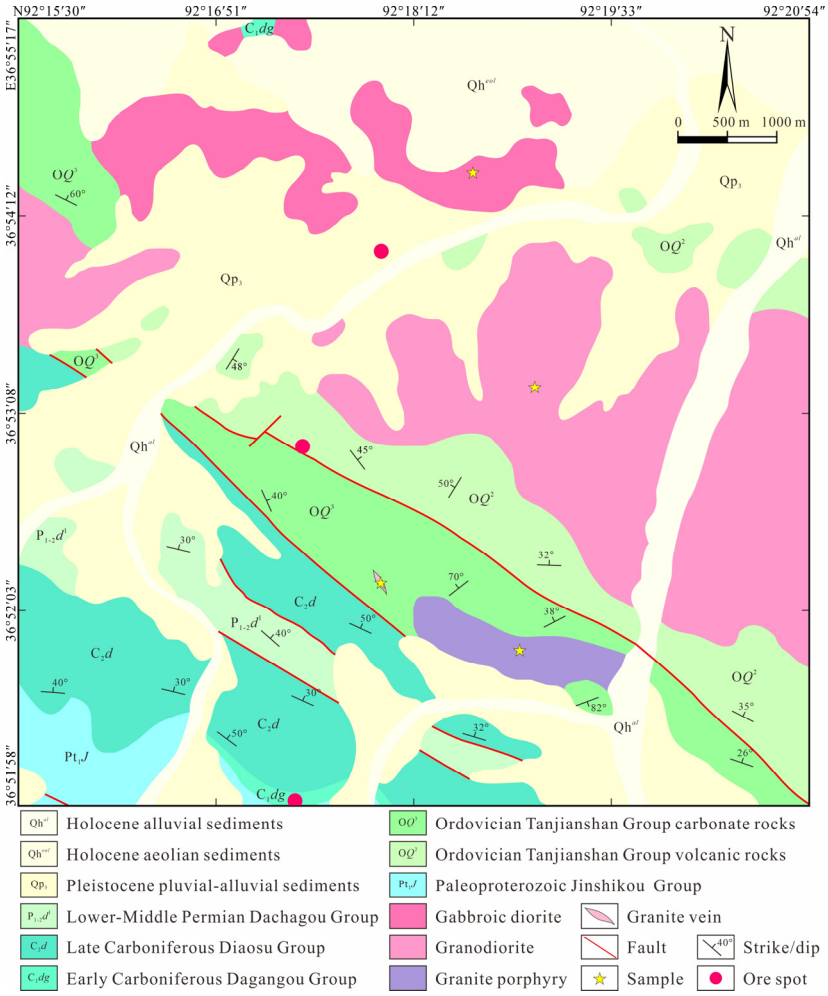


Figure 2. Geological map of the Niukutoudong deposit.

In summary, the Niukutoudong deposit occupies a strategically important position within the Early Paleozoic tectono-magmatic belt of the East Kunlun area. The widespread Early Devonian intermediate–felsic intrusive rocks, spatially and temporally associated with mineralization, constitute an ideal target for unraveling the genetic mechanisms and tectonic setting of this magmatism, as well as its links to regional tectonic evolution and metallogenesis.



Figure 3. Representative hand specimen photographs and photomicrographs showing intrusive rocks from the Niukutoudong deposit: (**a**–**c**) granite porphyry; (**d**–**f**) granodiorite; (**g**–**i**) granite; (**j**–**l**) gabbroic diorite. (**a**,**d**,**g**,**j**) hand specimen; (**b**,**e**,**h**,**k**) microscopic photos under plane-polarized light; (**c**,**f**,**i**,**l**) microscopic photos under cross-polarized light. Abbreviations of minerals: Hbl: hornblende; Qtz: quartz; Pl: plagioclase; Bt: biotite; Afs: Alkali feldspar; Cal: Calcite; Chl: Chlorite.

3. Sample Preparation and Analytical Methods

To precisely constrain the emplacement ages and unravel the petrogenesis of the Niukutoudong intrusive rocks, systematic zircon U-Pb geochronology and whole-rock major and trace element geochemical analyses were conducted on representative samples of granite porphyry, granodiorite, granite, and gabbroic diorite. Four intrusive rock samples were selected for zircon U-Pb dating, and 20 samples (5 samples per rock type) were selected for whole-rock major and trace element geochemical analyses. All analyses were conducted at accredited national and provincial key laboratories. The detailed analytical procedures and quality control protocols are outlined below.

3.1. Zircon Sorting, Target Preparation, and Cathodoluminescence (CL) Imaging

Four fresh rock samples (each with a mass of 5–10 kg) intended for geochronological dating were initially crushed using a jaw crusher and subsequently pulverized in a disk mill to approximately 200 mesh. Zircon crystals were isolated through conventional heavy-liquid and magnetic separation, and grains displaying euhedral morphology, high transparency and an absence of visible fractures and inclusions were then handpicked under a binocular microscope. The selected zircons were embedded in epoxy resin and polished to expose their internal surfaces, yielding grain mounts. Prior to analysis, the mounts were ultrasonically cleaned in a 3% HNO_3 solution to remove surface contaminants. To visualize internal structures and select optimal analytical targets, all zircon grains were imaged by cathodoluminescence (CL) using a scanning electron microscope equipped with a CL detector.

3.2. Zircon U-Pb Dating

Zircon U–Pb geochronological analyses were performed at the Key Laboratory of Mineral Resource Evaluation in Northeast Asia, Ministry of Natural Resources. A GeoLasPro 193 nm ArF excimer laser ablation system (Santa Clara, CA, USA) coupled to an Agilent 7900 (Santa Clara, CA, USA) inductively coupled plasma mass spectrometer (ICP-MS) was used for the analyses.

High-purity helium was used as the carrier gas to transport the ablated aerosol, which was mixed with argon prior to introduction into the ICP-MS. Laser ablation was performed in single-spot mode with a spot diameter of 32 μm, a repetition rate of 10 Hz, and a fluence of approximately 8 J/cm^2. Each analysis consisted of approximately 20 s of background acquisition and 40 s of signal collection. Elemental fractionation was corrected by external standardization using the Plešovice zircon standard (337.13 ± 0.37 Ma; [62]), with two Plešovice analyses performed after every five unknown spot measurements. The 91,500 zircon (1065.4 ± 0.6 Ma; [63]) was employed as a quality-control monitor. During this analytical session, it yielded a weighted mean $^{206}Pb/^{238}U$ age of 1063 ± 5 Ma (MSWD = 0.8, n = 12), which is consistent within uncertainty with the recommended value, confirming the reliability of the data.

Raw data were processed offline using ICPMSDataCal 10.8 (the State Key Laboratory of GPMR, China University of Geosciences, Wuhan, China) [64], and common Pb correction was performed following the method of [65]. Age calculations and concordia diagrams were constructed using Isoplot 4.15 (the Berkeley Geochronology Center, Berkeley, CA, USA) [66]. All ages reported herein are $^{206}Pb/^{238}U$ ages, and the weighted mean age with its 95% confidence interval is taken as the emplacement age of the intrusive rock.

3.3. Whole-Rock Major and Trace Elements

All samples selected for whole-rock geochemical analysis were fresh, unaltered drill core or hand specimens. They were thoroughly washed with deionized water, dried, and then ground to <200 mesh in a contamination-free laboratory using a high-purity alumina ceramic jaw crusher and an agate mill.

Major element analyses were performed at the Key Laboratory of Mineral Resource Evaluation in Northeast Asia, Ministry of Natural Resources. Approximately 1.0 g of sample powder was oven-dried at 105 °C and subsequently ignited in a muffle furnace at 1000 °C for two hours to determine loss on ignition (LOI). The ignited powder was mixed with lithium tetraborate flux (sample:flux = 1:10) and fused at 1150 °C to produce homogeneous glass disks. Measurements were conducted using a Rigaku ZSX Primus II wavelength-dispersive X-ray fluorescence spectrometer. Data quality was monitored by repeated analyses of the Chinese national rock reference materials GB07103 and GB07105, which yielded results in excellent agreement with the recommended values. Detection limits were 0.015% for Al_2O_3, SiO_2, MgO, and Na_2O; 0.01% for CaO, K_2O, TiO_2, and total $Fe_2O_3{}^T$; and 0.005% for MnO and P_2O_5. The ferrous iron (FeO) content was determined by volumetric titration, with a detection limit of 0.1%. Trace element (including rare earth elements) analyses were carried out in the same laboratory using an Agilent 7500 inductively coupled plasma mass spectrometer (ICP-MS).

The digestion protocol was as follows: approximately 50 mg of powder was accurately weighed into Teflon bombs, to which 1 mL of high-purity HNO_3 and 1 mL of high-purity HF were added. The sealed bombs were heated at 190 °C for more than 48 h. After evaporation to dryness, 1 mL of HNO_3 was added and again evaporated to dryness to expel residual HF. The residue was finally taken up in 2% HNO_3 and diluted to 100 mL. Rhodium was used as an internal standard to correct for instrumental drift. The reference materials GB07103 and GB07105 were analyzed as quality-control monitors; the measured

concentrations of the vast majority of elements deviated from the recommended values by less than 5%, confirming the accuracy and reliability of the data.

4. Results

4.1. Zircon U-Pb Ages

Zircon U-Pb age and trace element data are presented in Supplementary Table S1. Representative CL images, concordia diagrams, and weighted mean age plots are shown in Figure 4.

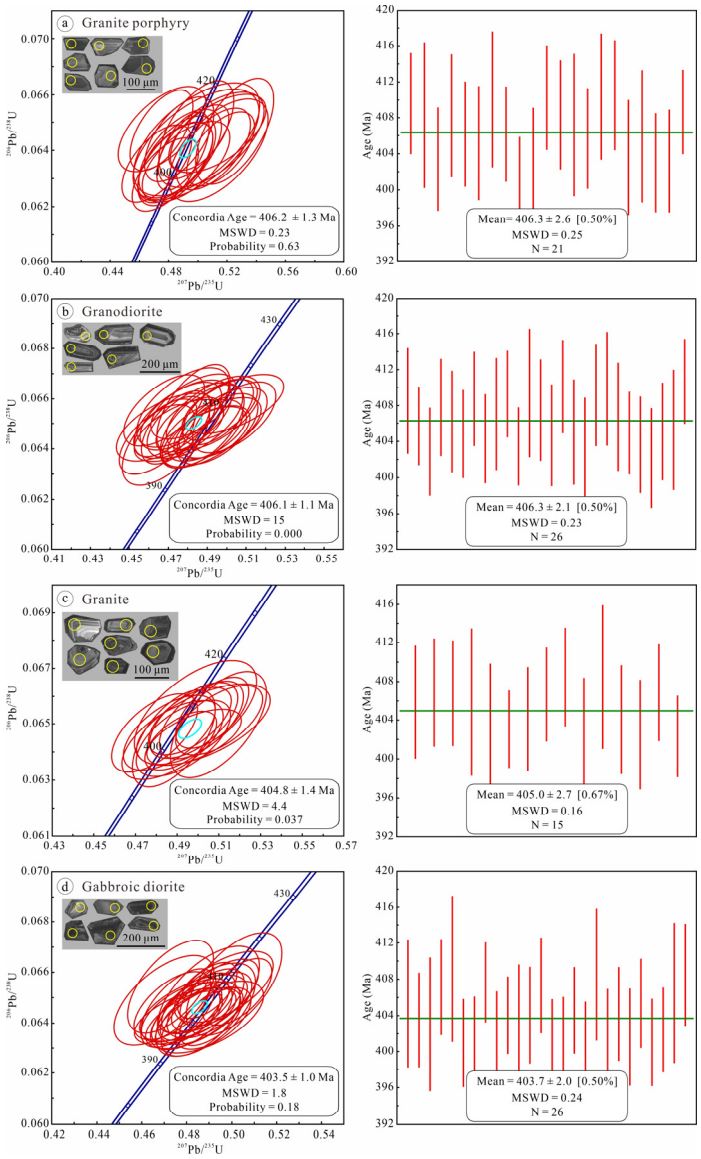


Figure 4. Representative CL images, zircon U-Pb concordia diagrams and weighted average ages diagrams. (**a**) The results of the granite porphyry sample; (**b**) the results of the granodiorite sample; (**c**) the results of the granite sample; (**d**) the results of the gabbroic diorite sample.

All analyzed zircon grains are euhedral to subhedral and display well-developed magmatic oscillatory zoning (Figure 4). Their Th/U ratios (0.12–2.67) are consistently high, consistent with magmatic origin (Th/U > 0.1). All analytical spots plot on or near the concordia curve, indicating that the zircon U-Pb system remained closed and was not perceptibly disturbed by post-crystallization thermal events.

Twenty-one analytical spots of granite porphyry yield a weighted average $^{206}Pb/^{238}U$ age of 406.3 ± 2.6 Ma (MSWD = 0.25) and a concordia age of 406.2 ± 1.3 Ma (Figure 4a). Twenty-six analytical spots of granodiorite yield a weighted average $^{206}Pb/^{238}U$ age of 406.3 ± 2.1 Ma (MSWD = 0.23) and a concordia age of 406.1 ± 1.1 Ma (Figure 4b). Fifteen analytical spots of granite yield a weighted average $^{206}Pb/^{238}U$ age of 404.8 ± 1.1 Ma (MSWD = 0.16) and a concordia age of 405.0 ± 2.7 Ma (Figure 4c). Twenty-six analytical spots of gabbroic diorite yield a weighted average $^{206}Pb/^{238}U$ age of 403.7 ± 2.0 Ma (MSWD = 0.24) and a concordia age of 403.5 ± 1.0 Ma (Figure 4d).

Collectively, the emplacement ages of the granite porphyry, granodiorite, granite, and gabbroic diorite in the Niukutoudong deposit are tightly clustered between 403.7 and 406.3 Ma, corresponding to the Early Devonian.

4.2. Whole-Rock Geochemistry

4.2.1. Major Element Geochemistry

Major element data of the intrusive rocks in the Niukutoudong deposit are presented in Supplementary Table S2.

All samples have Rittmann index ($\sigma = [w(Na_2O) + w(K_2O)]^2/[w(SiO_2) - 43\%]$) of 0.77–2.74, consistently below 3.3, indicating a calc-alkaline affinity. They all plot within the subalkaline field on the TAS diagram (Figure 5a). Based on their SiO_2 contents and normative mineralogy, the samples are classified as gabbroic diorite, granodiorite, and granite, in full agreement with their petrographic designations. On the SiO_2 vs. K_2O diagram (Figure 5c), all samples fall within the high-K calc-alkaline series. A pronounced trend of increasing K_2O with SiO_2 is evident from the intermediate gabbroic diorite to the felsic granite porphyry. On the AFM diagram (Figure 5b), the data points follow a calc-alkaline differentiation trend. Aluminum saturation index (A/CNK) values indicate that the granite porphyry and granite are weakly peraluminous (A/CNK = 1.16–1.32 and 0.98–1.10, respectively), whereas the granodiorite and gabbroic diorite are metaluminous (A/CNK = 0.87–0.99 and 0.82–0.89, respectively; Figure 5d).

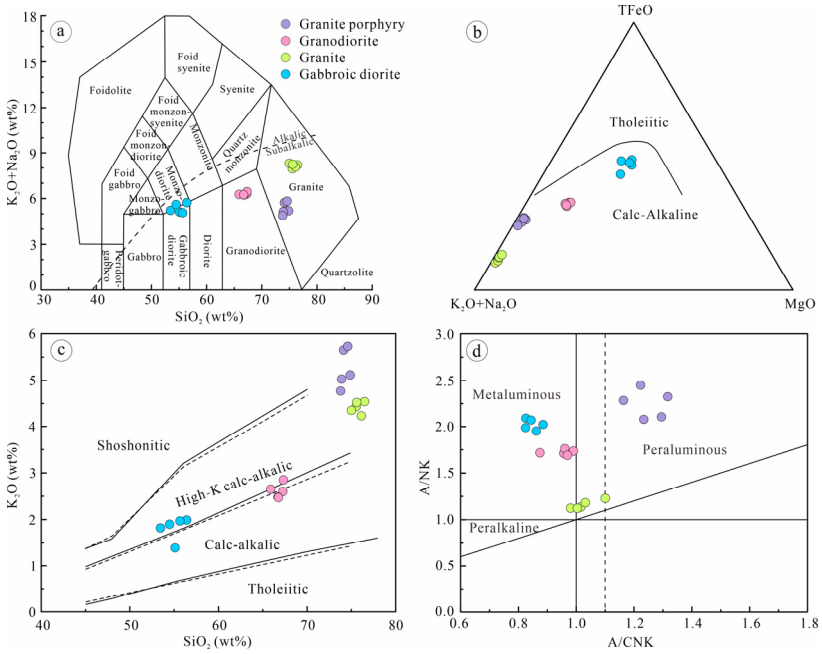


Figure 5. Geochemical diagrams of intrusive rocks from the Niukutoudong deposit. (**a**) SiO_2 vs. $K_2O + Na_2O$ [67]; (**b**) TFeO–$K_2O + Na_2O$–MgO [68]; (**c**) SiO_2 vs. K_2O [69]; (**d**) A/CNK vs. A/NK [70].

In summary, the major element geochemistry delineates a continuous compositional spectrum from intermediate to felsic lithologies, and the suite as a whole belongs to a high-K calc-alkaline, metaluminous to weakly peraluminous series.

4.2.2. Rare Earth and Trace Element Geochemistry

Rare earth element (REE) and trace element data for the intrusive rocks in the Niukutoudong deposit are listed in Supplementary Table S2. The chondrite-normalized REE patterns and primitive mantle-normalized trace element spider diagrams are shown in Figure 6. All samples exhibit remarkably consistent REE patterns characterized by enrichment in light rare earth elements (LREEs) and relatively flat heavy rare earth elements (HREEs), forming right-sloping curves (Figure 6a). La_N/Yb_N ratios range from 3.91 to 8.94, indicating moderate LREE/HREE fractionation. All samples display negative Eu anomalies, which range from weak to pronounced. The gabbroic diorite (δEu = 0.77–0.89) and granodiorite (δEu = 0.81–0.87) display weak negative Eu anomalies, whereas the granite (δEu = 0.15–0.26) and granite porphyry (δEu = 0.52–0.58) exhibit pronounced negative Eu anomalies. Total REE concentrations (ΣREE) vary widely, from ~80 ppm in the granodiorite and granite to ~280 ppm in the granite porphyry.

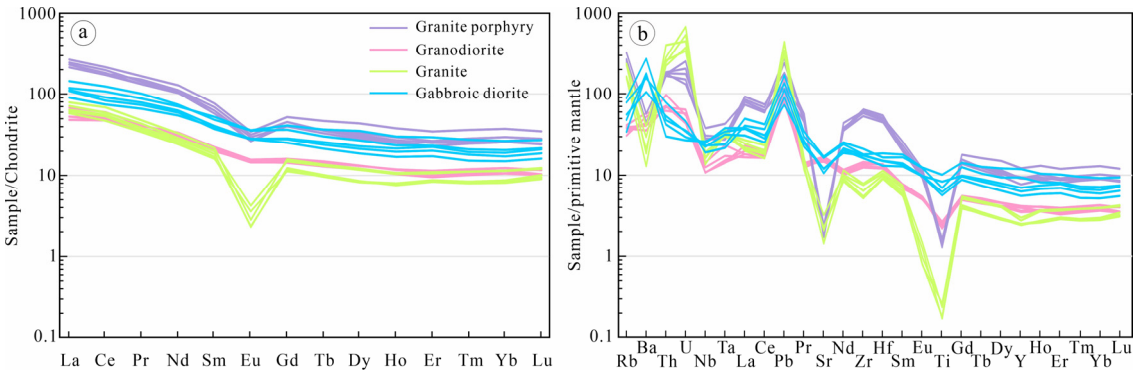


Figure 6. Chondrite-normalized REE pattern (**a**) and primitive mantle-normalized trace element spider diagram (**b**) of intrusive rocks in the Niukutoudong deposit. The values of primitive mantle and chondrite are from [71].

On the primitive mantle-normalized trace element spider diagram (Figure 6b), granite, granodiorite, and gabbro exhibit similar distribution patterns, characterized by enrichment in large ion lithophile elements (LILEs, e.g., Rb, Ba, Pb) and depletion in high field strength elements (HFSEs, e.g., Nb, Ta, Ti). By contrast, granite porphyry is similarly enriched in LILEs, and displays high abundances of HFSEs (Zr + Ce + Nb + Y).

Notably, source-sensitive incompatible element ratios (e.g., Nb/Ta, La/Nb) show narrow variations across the different lithologies and plot between typical mantle and crustal values (see Discussion), suggesting a complex source.

5. Discussion

5.1. Petrogenesis and Magma Source

Granitoids are genetically subdivided into I-, S-, and A-types on the basis of their source-rock characteristics [72–77]. Discrimination diagrams (Figure 7) indicate that granite porphyry plots within the A-type field, whereas granite, granodiorite, and gabbroic diorite fall into the I- and S-type fields.

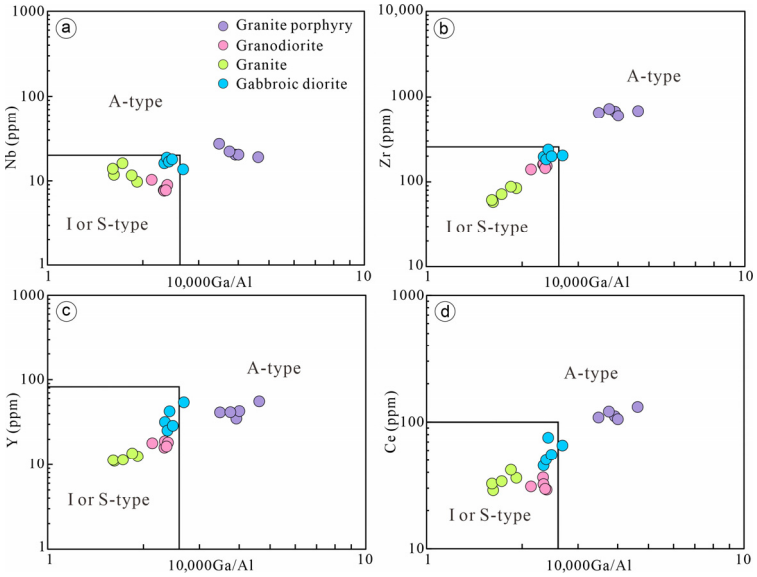


Figure 7. The discrimination diagrams of intrusive rocks from the Niukutoudong deposit. (**a**–**d**) Nb, Zr, Y and Ce vs. 10,000 × Ga/Al, respectively [78].

Granite porphyry is distinguished by elevated K_2O (4.77–5.73 wt%), high total rare earth element contents (ΣREE = 256.12–323.56 ppm, average 280.66 ppm), and notably high abundances of HFSEs (Zr + Ce + Nb + Y = 766.23–906.48 ppm, averaging 845.38 ppm, <350 ppm), further substantiating an A-type affinity [79].

In contrast, granite, granodiorite, and gabbroic diorite exhibit markedly lower HFSE abundances (Zr + Ce + Nb + Y = 109.91–373.67 ppm, averaging 219.42 ppm, i.e., <350 ppm). This clearly distinguishes them from typical A-type granites and necessitates discrimination between I- and S-type affinities. S-type granites are mineralogically characterized by the presence of peraluminous phases such as garnet, muscovite, and cordierite, and by the typical absence of hornblende [80]. The studied samples lack such peraluminous minerals, and their average A/CNK ratio is 1.01 (<1.10), inconsistent with S-type signatures. During fractional crystallization, the solubility of apatite decreases with increasing SiO_2 in I-type granitic magmas but follows the opposite trend in S-type systems [81]. Granite, granodiorite, and gabbroic diorite exhibit a clear decrease in P_2O_5 with increasing SiO_2 (Figure 8a), strongly supporting an I-type origin. Furthermore, on Rb vs. Y and Rb vs. Th diagrams (Figure 8c,d), these samples exhibit positive correlations of Th and Y with Rb, following I-type evolutionary trends. Consequently, the Niukutoudong granite, granodiorite, and gabbroic diorite are classified as I-type granitoids.

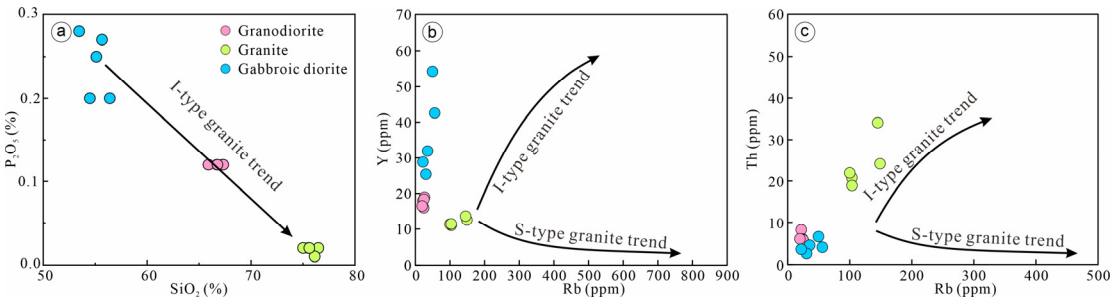


Figure 8. The discrimination diagrams of intrusive rocks from the Niukutoudong deposit. (**a**) SiO_2 vs. P_2O_5; (**b**,**c**) Yb and Th vs. Rb, respectively [82].

Petrogenetic models for I-type granitoids converge on two principal mechanisms: (1) crustal anatexis triggered by the underplating of differentiated mantle-derived

melts [83–86] and (2) mixing between upwelling mantle-derived magmas and crust-derived felsic magmas, producing mixed magmas that subsequently undergo fractional crystallization [87]. A-type granites may be produced by extreme fractional crystallization of mantle-derived basaltic magmas [74], partial melting of crustal sources [88,89], or crust–mantle mixed magma [77].

Regarding rare earth elements, all samples display right-sloping patterns characterized by LREE enrichment and relatively flat HREEs (La_N/Yb_N = 3.91–8.84, average 6.55), along with weak or pronounced negative Eu anomalies (δEu = 0.15–0.89, average 0.60). These signatures suggest that plagioclase persisted as a stable residual phase whereas garnet was largely consumed, implying derivation from a shallow, low-pressure source [90], and that the magmas underwent plagioclase fractionation during ascent or ponding.

Previous Hf isotopic studies on coeval intrusive rocks in the adjacent Niukutou and Yemaquan districts have demonstrated that these plutons originated through crust–mantle magma mixing [20,54]. Regionally, other contemporaneous intrusive rocks similarly exhibit mixed crust–mantle source signatures [12,14,16,21,32,48,50]. Thus, a mixed crust–mantle origin emerges as a pervasive characteristic of coeval magmatism across the region.

In addition, some elemental ratios could indicate the compositions of the rock. The reference values for Nb/Ta, Ba/Nb, and La/Nb are 12, 54.0, and 2.20, respectively, for the continental crust and 17.5, 9.0, and 0.94 for the mantle [71,91,92]. In the study area, granite porphyry exhibits average Nb/Ta ratios (16.87), approaching the upper-mantle value (17.5), while its average Ba/Nb and La/Nb ratios (14.98 and 2.64) fall between crustal and mantle end-members, collectively pointing to a mixed source dominated by mantle components. Granodiorite and granite yield average Nb/Ta ratios (12.35 and 9.45) close to the typical crustal value (12), and their Ba/Nb ratios (38.84 and 14.72) and La/Nb ratios (1.60 and 1.30) display transitional crust–mantle characteristics, indicating a more significant crustal contribution—potentially resulting from mixing of mantle-derived magmas with crustal melts or from partial melting of mafic lower crust. Gabbroic diorite records average Nb/Ta ratios (13.82) intermediate between crustal (12) and mantle (17.5) values, and its average La/Nb ratios (1.65) similarly straddle the two, attesting to a mixed crust–mantle source.

Taken together, the source attributes of coeval regional intrusive rocks and the incompatible-element ratios presented above imply that the Niukutoudong intrusive rocks are likely products of crust–mantle interaction, with the different lithologies reflecting variable mixing proportions between the two end-members.

In summary, the Niukutoudong intrusive rocks display petrographic and geochemical characteristics diagnostic of I-type or A-type granitoids. Their genesis is best explained by mixing of crust- and mantle-derived magmas, followed by fractional crystallization of K-feldspar and plagioclase during magmatic evolution, ultimately producing the intrusive rocks exposed in the study area.

5.2. Tectonic Setting: Evidence of Post-Collisional Extensional Setting in the Early Devonian

Zircon U-Pb geochronology demonstrates that the granite porphyry, granodiorite, granite, and gabbroic diorite in the Niukutoudong deposit were emplaced at 406.3 ± 2.6 Ma, 406.3 ± 2.1 Ma, 405.0 ± 2.7 Ma and 403.7 ± 2.0 Ma, respectively, all within the Early Devonian. These intrusive rocks are uniformly enriched in LILEs and depleted in HFSEs, with geochemical characteristics of volcanic-arc granites [89].

Based on Sr and Yb contents, a petrogenetic classification of granitoids was proposed, linking formation pressure to tectonic setting, and subdivided granites into high-Sr low-Yb, low-Sr low-Yb, high-Sr high-Yb, low-Sr high-Yb (Sr < 400 ppm, Yb > 2 ppm), and very low-Sr high-Yb types [93]. The intrusive rocks in the study area have Sr contents of 30.20–360.52 ppm (average 177.78 ppm) and Yb contents of 1.37–6.40 ppm (average

2.98 ppm), matching the low-Sr, high-Yb granite category. This type typically forms at pressures below 1 GPa and exhibits distinct or weak negative Eu anomalies [93], indicating generation in an extensional post-collisional regime. Post-collisional stress relaxation and lithospheric delamination or thinning induce asthenospheric upwelling and melting of enriched mantle, thereby creating the requisite conditions for crust–mantle interaction. The mixed crust–mantle source signature of the Niukutoudong intrusive rocks further supports a post-collisional extensional setting. On the Y + Nb vs. Rb and Y vs. Nb tectonic discrimination diagrams (Figure 9), most samples plot within the post-collisional field, consistent with the geochemical inferences above. This finding aligns with the regional Late Silurian–Middle Devonian post-collisional tectonic framework in the East Kunlun area [46].

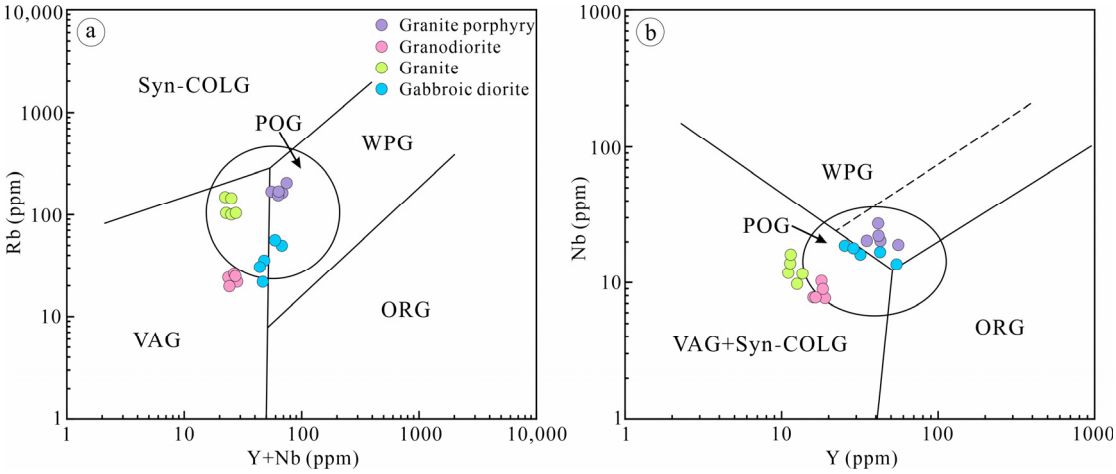


Figure 9. Diagrams for discriminating the tectonic setting of granites. (**a**) Y + Nb vs. Rb [94]; (**b**) Y vs. Nb [95]. Syn-COLG: syn-collisional granites; POG: post-collisional granites; WPG: within-plate granites; VAG: volcanic arc granites; ORG: ocean ridge granites.

Collectively, the Early Devonian Niukutoudong intrusive rocks were emplaced in a post-collisional extensional setting.

5.3. Insights into the Early Paleozoic Tectonic Evolution of the East Kunlun Orogenic Belt

During the Early Paleozoic, the East Kunlun Orogenic Belt underwent a complete Caledonian tectonic cycle that encompassed the formation and expansion of Proto-Tethys oceanic crust, subduction and consumption, collisional to post-collisional orogeny, and post-orogenic collapse and uplift [96–98]. By integrating previously published data, this study systematically summarizes the emplacement ages, tectonic settings, and spatial distribution of plutons across the belt, and on this basis constructs a simplified tectonic evolutionary sequence diagram for the Early Paleozoic Proto-Tethys Ocean in the belt (Figure 10).

The Early Cambrian marked the opening and expansion of the Proto-Tethys Ocean [7]. At approximately 520 Ma, the Proto-Tethys Ocean began to subduct southward [8,9], and subduction persisted into the Late Ordovician [53]. Subduction-related magmatism, exemplified by the Aquedun monzogranite (448.8 Ma [18]), the Xiarihamu diorite porphyrite (441.1 Ma [23]), and the Dagele ophiolite gabbro (445 Ma [37]), indicates that subduction may have continued until 441–448 Ma, with earlier cessation in the eastern segment. The appearance of the Tumuluke gabbro at 444.5 Ma may represent the end of subduction and the onset of collision [1]. Syn-collisional Bashierxi S-type granites (433.2 Ma, 432 Ma, and 431.3 Ma [43]) and the Dagele gabbro (430.2 Ma [40]) further demonstrate that the collisional stage continued until ca. 430 Ma.

From ca. 430 Ma onward, a succession of extension-related plutons emerged in the region, including the Xialaganuo A-type granite (430.1 Ma [19]), the Kaerqueka A-type granite (425 Ma [15]), the Kunlunhe S-type granites (427.9 Ma and 432.6 Ma [31]), the Haidewula A-type granite (422 Ma [51]), the Dachaigou I-type granite (417.4 Ma [50]), and the Niukutoudong I-type granites (~405 Ma, this study). The temporal progression of these plutonic associations reveals a transformation from predominantly crustal melting (S-type) to mixed crust–mantle sources (I-type) at ~430 Ma. This transformation records the thermo-mechanical transition from lithospheric thickening under compression to thinning during extension. Accordingly, the East Kunlun region progressively evolved from a collisional compressional regime into a post-collisional extensional setting, beginning in the Late Silurian (ca. 430 Ma).

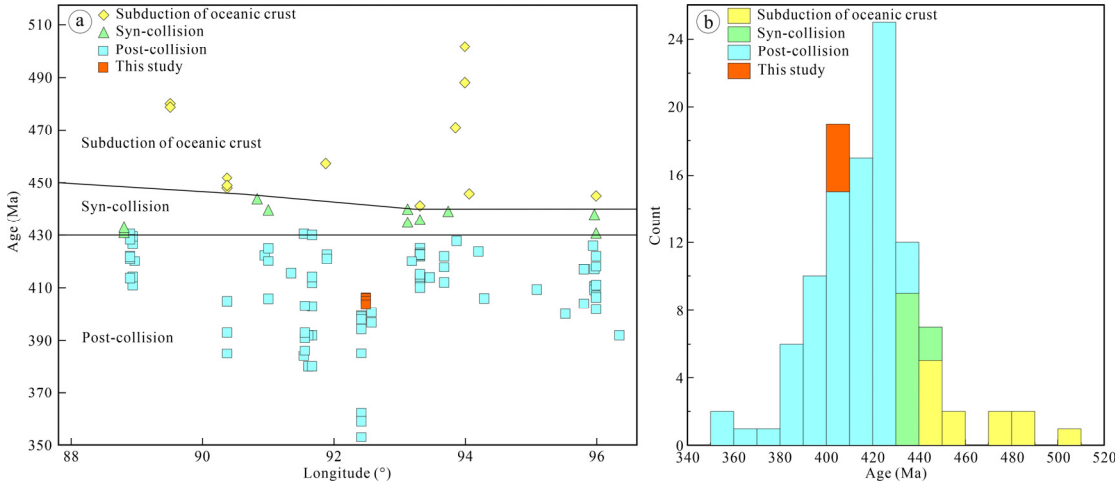


Figure 10. Schematic diagram of the Early Paleozoic tectono-magmatic event sequence in the western segment of the East Kunlun Orogenic Belt. Age data are from [1,11–53] and references therein. (**a**) Plot of age vs. longitude and (**b**) histogram of age distribution for magmatic rocks of different tectonic stages.

The absence of Lower–Middle Devonian strata, the widespread occurrence of Upper Devonian continental molasse, and its regional unconformable contact on Early Paleozoic and older sequences and geological bodies collectively provide indirect evidence that the East Kunlun Orogenic Belt had entered a post-orogenic collapse stage by the Late Devonian, marking the onset of a new orogenic cycle [1].

In summary, this systematic tectono-magmatic evolutionary sequence records a complete Wilson cycle of the East Kunlun Proto-Tethys Ocean—from expansion, subduction, and closure to extension—and provides critical constraints on the Early Paleozoic orogenic processes and the geodynamic mechanisms of the Proto-Tethys tectonic domain.

5.4. Insights into the Qimantage Polymetallic Metallogenic Belt

The Qimantage polymetallic metallogenic belt in the East Kunlun area hosts more than 30 porphyry–skarn deposits, predominantly of small to medium scale, all of which formed during the collisional stages following the closures of the Proto-Tethys and Paleo-Tethys Oceans (435–370 Ma and 245–196 Ma, respectively; [99–105]). Although the Qimantage region has long been celebrated as a classic example of a Triassic metallogenic explosion [106], the Silurian–Devonian (the collision stage of the Proto-Tethys Ocean) mineralization potential is equally compelling. During the Silurian–Devonian collision following the closure of the Proto-Tethys Ocean, slab break-off and post-collisional extension induced large-scale asthenospheric upwelling [107,108]. As mantle-derived magmas ascended, they interacted to varying degrees with continental crustal materials, becoming enriched in ore-forming

elements and ultimately forming various types of ore deposits in the upper crust [106] (Figure 11).

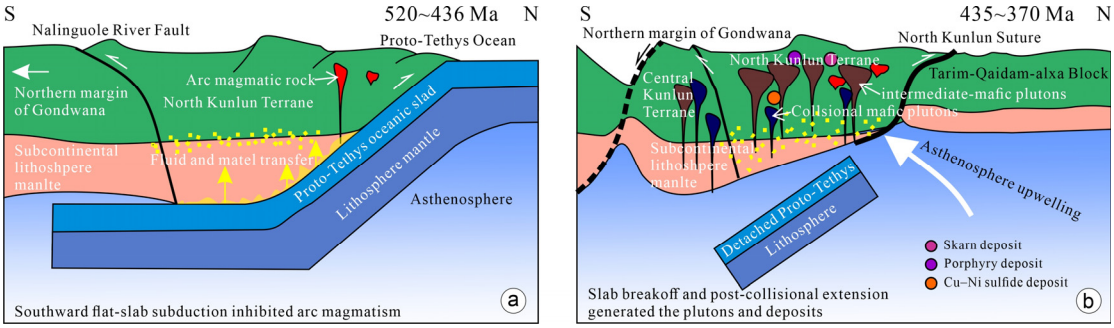


Figure 11. Schematic cartoon showing the tectonic evolution and mineralization of the Qimantag metallogenic belt in the East Kunlun Orogenic Belt (Modified from [106]).

In recent years, magmatic–metallogenic events of this episode have been increasingly documented in other segments of the East Kunlun Orogenic Belt. For example, Silurian–Devonian intrusions derived from crust–mantle mixing and associated Cu–Au and Pb–Zn mineralization have been successively identified in the Gouli and Wulonggou districts [109–113]. Although these occurrences differ in tectonic setting and deposit type, they all lie within the same post-collisional extensional geodynamic framework following the closure of the Proto-Tethys Ocean. This demonstrates that crust–mantle interaction exerted a pervasive control on mineralization across the entire belt within the Silurian–Devonian post-collisional extensional regime.

The Niukutoudong cobalt polymetallic deposit is situated within this tectono-magmatic setting. The intimate spatiotemporal association between mineralization and the ~405 Ma mixed crust–mantle I-type granites revealed by this study is far from coincidental. Such mixed magmas are typically characterized by high oxygen fugacity and elevated volatile contents (e.g., F, Cl, CO_2) [114,115]. Niukutoudong intrusive rocks have an average zircon oxygen fugacity of ΔFMQ +1.27. These conditions are highly favorable for extracting and transporting metal elements such as Co, Cu, and Au from the magma source [114,115]. Research by [116–119] has also demonstrated the considerable metallogenic potential of these magmatic–hydrothermal systems.

Accordingly, we propose that the polymetallic mineralization at the Niukutoudong deposit is most likely directly linked to the Early Devonian mixed crust–mantle magmatism and its derivative hydrothermal system identified in this work. This magmatism not only provided some of the metals and the thermal energy required for mineralization, but also created optimal ore-forming conditions through its distinctive physicochemical characteristics. This insight opens a significant new exploration direction in the Qimantage belt, targeting coeval (~405 Ma) I-type granitoid intrusive rocks.

6. Conclusions

(1) Zircon U-Pb geochronology shows that the Niukutoudong intrusive rocks were formed at 406.3–403.7 Ma, i.e., in the Early Devonian.

(2) Geochemically, granite, granodiorite, and gabbroic diorite are high-K calc-alkaline, metaluminous to weakly peraluminous I-type granitoids, and granite porphyry is peraluminous A-type granitoids. Their elemental compositions reveal a mixed source involving both crustal and mantle components.

(3) Combined with regional tectonic constraints, these geochemical features indicate that the intrusive rocks formed in a post-collisional extensional setting following the closure of the Proto-Tethys Ocean and the cessation of syn-collisional convergence.

They thus constitute a key magmatic record of the East Kunlun Orogenic Belt's transition from compressional thickening to extensional thinning.

(4) This crust–mantle mixing magmatism is likely genetically linked to the Niukutoudong cobalt polymetallic mineralization, providing a new tectono-magmatic perspective on the regional metallogenic framework of the Qimantage belt.

Supplementary Materials: The following supporting information can be downloaded at: https://www.mdpi.com/article/10.3390/min16080772/s1, Table S1. Ziron U-Pb age and trace element data from intrusive rocks in the Niukutoudong deposit. Table S2. Whole-rock major, trace element data of intrusive rocks in the Niukutoudong deposit.

Author Contributions: Conceptualization, X.X.; Methodology, X.X. and Y.Q.; Validation, J.Y.; Formal analysis, S.J.; Investigation, Y.J., S.C., W.Z., D.Y., S.J. and Y.Q.; Resources, X.L.; Data curation, X.X., W.Z. and D.Y.; Writing—original draft, X.X.; Writing—review & editing, Y.J. and Y.Q.; Supervision, S.C. and J.Y.; Project administration, X.L. All authors have read and agreed to the published version of the manuscript.

Funding: This research received support from the Young and Middle-aged Science and Technology Talent Support Project of Qinghai Association for Science and Technology (2024QHSKXRCTJ48) and the Open Research Project of the Qinghai Provincial Key Laboratory of Buried Ore Exploration (Grant No. 2025qhyfkf03).

Data Availability Statement: Data are contained within the article and Supplementary Materials.

Acknowledgments: We thank the editors and two anonymous reviewers for their constructive comments which helped in improving our manuscript.

Conflicts of Interest: The authors declare no conflicts of interest.

References

1. Mo, X.X.; Luo, Z.H.; Deng, J.F.; Yu, X.H.; Liu, C.D.; Chen, H.W.; Yuan, W.M.; Liu, Y.H. Granitoids and crustal growth in the East-Kunlun Orogenic Belt. *Geol. J. China Univ.* **2007**, *13*, 403–414. (In Chinese with English abstract)
2. Feng, D.; Wang, C.; Song, S.G.; Xiong, L.; Zhang, G.B.; Allen, M.B.; Dong, J.; Wen, T.; Su, L. Tracing tectonic processes from Proto- to Paleo-Tethys in the East Kunlun Orogen by detrital zircons. *Gondwana Res.* **2023**, *115*, 1–16. [CrossRef]
3. Bian, Q.T.; Li, D.H.; Pospelov, I.; Yin, L.M.; Li, H.S.; Zhao, D.S.; Chang, C.F.; Luo, X.Q.; Gao, S.L.; Astrakhantsev, O.; et al. Age, geochemistry and tectonic setting of Buqingshan ophiolites, North Qinghai-Tibet Plateau, China. *J. Asian Earth Sci.* **2004**, *23*, 577–596. [CrossRef]
4. Chen, J.J.; Fu, L.B.; Wei, J.H.; Selby, D.; Zhang, D.H.; Zhou, H.Z.; Zhao, X.; Liu, Y. Proto Tethys magmatic evolution along northern Gondwana: Insights from late Silurian Middle Devonian A-type magmatism, East Kunlun Orogen, Northern Tibetan Plateau, China. *Lithos* **2020**, *356–357*, 105304. [CrossRef]
5. Mattern, F.; Schneider, W.; Li, Y.; Li, X. A traverse through the western Kunlun (Xinjiang, China): Tentative geodynamic implications for the Paleozoic and Mesozoic. *Geol. Rundsch.* **1996**, *85*, 705–722. [CrossRef]
6. Chen, J.J.; Wei, J.H.; Fu, L.B.; Li, H.; Zhou, H.Z.; Zhao, X.; Zhan, X.F.; Tan, J. Multiple sources of the early Mesozoic Gouli batholith, Eastern Kunlun Orogenic Belt, northern Tibetan Plateau: Linking continental crustal growth with oceanic subduction. *Lithos* **2017**, *292–293*, 161–178. [CrossRef]
7. Yang, J.S.; Robinson, P.T.; Jiang, C.F.; Xu, Z.Q. Ophiolites of the Kunlun Mountains, China and their tectonic implications. *Tectonophysics* **1996**, *258*, 215–231. [CrossRef]
8. Li, S.Z.; Zhao, S.J.; Liu, X.; Cao, H.H.; Yu, S.; Li, X.Y.; Somerville, I.; Yu, S.Y.; Suo, Y.H. Closure of the Proto-Tethys Ocean and Early Paleozoic amalgamation of microcontinental blocks in East Asia. *Earth-Sci. Rev.* **2018**, *186*, 37–75. [CrossRef]
9. Song, S.G.; Bi, H.Z.; Qi, S.S.; Yang, L.M.; Allen, M.B.; Niu, Y.L.; Su, L.; Li, W.F. HP–UHP metamorphic belt in the East Kunlun Orogen: Final closure of the Proto-Tethys Ocean and formation of the Pan-North-China Continent. *J. Petrol.* **2018**, *59*, 2043–2060. [CrossRef]
10. Dong, Y.P.; He, D.F.; Sun, S.S.; Liu, X.M.; Zhou, X.H.; Zhang, F.F.; Yang, Z.; Cheng, B.; Zhao, G.C.; Li, J.H. Subduction and accretionary tectonics of the East Kunlun Orogen, western segment of the Central China Orogenic System. *Earth-Sci. Rev.* **2018**, *186*, 231–261. [CrossRef]

11. Wang, Z.Z.; Han, B.F.; Feng, C.Y.; Li, G.C. Geochronology, geochemistry and tectonic significance of granites in Baiganhu area, Xinjiang. *Acta Petrol. Mineral.* **2014**, *33*, 597–616. (In Chinese with English abstract)
12. Wang, Y.F.; Li, M.; Zha, X.F.; Hu, C.B.; Li, Y.; Gao, X.F. Origin of granites from A'quedun Area in Qimantage Mountains: Constraints from zircon U-Pb dating, geochemistry and Hf isotope. *Earth Sci.* **2018**, *43*, 4319–4333. (In Chinese with English abstract)
13. Wu, S.K.; Zhang, H.; Zhang, L.H.; Miao, G.W.; Wu, Z.Z.; Tang, Y.; Tian, T.; Qiao, J.F. Geochemical characteristics and petrogenesis of the Donggouxi alkaline complex rocks in East Kunlun. *Acta Petrol. Sin.* **2025**, *41*, 2759–2777. (In Chinese with English abstract) [CrossRef]
14. Wang, P.X.; Guo, F.; Wang, Z.N. Zircon U-Pb geochronology, geochemistry and geological significance of granitoids in the Yazigou Qimantage Area of East Kunlun Mountains. *Geoscience* **2020**, *34*, 987–1000. (In Chinese with English abstract)
15. Chen, H.F.; He, S.Y.; Zhang, A.K.; Sun, J.L.; Yan, Z.P.; Liu, J.L.; Zhang, L.; Qian, Y. Petrogenesis and tectonic setting of Middle Silurian A-type granite in Kaerqueka area, East Kunlun. *Geol. Bull. China* **2021**, *40*, 1380–1393. (In Chinese with English abstract)
16. . (In Chinese with English abstract) Hao, N.N.; Yuan, W.M.; Zhang, A.K.; Feng, Y.L.; Cao, J.H.; Chen, X.N.; Cheng, X.Q.; Mo, X.X. Evolution process of the Late Silurian–Late Devonian tectonic environment in Qimantagh in the western portion of east Kunlun, China: Evidence from the geochronology and geochemistry of granitoids. *J. Earth Syst. Sci.* **2015**, *124*, 171–196. [CrossRef]
17. Wang, Z.S.; Zhang, L.C.; Zhang, D.M.; Zhang, Y.; Lin, G.; Li, W. Characteristics and genesis analysis of the large fluorite deposit in Kayakedeng, East Kunlun: Constraints from Sm-Nd and U-Pb isotopes and geochemistry of rare earth elements. *Earth Sci.* **2026**, 1–22. (In Chinese with English abstract)
18. Li, T.; Li, M.; Hu, C.B.; Li, Y.; Meng, J.; Gao, X.F.; Zha, X.F. Zircon U-Pb geochronology, geochemistry and its geological implications of intrusions in Aquedun Area from Qimantag, East Kunlun, China. *Earth Sci.* **2018**, *43*, 4350–4363. (In Chinese with English abstract)
19. Xu, B.; Tong, H.K.; Liu, B.; Liu, L.S. Discovery and tectonic significance of Mid-Silurian rapakivi granites and hornblende-gabbros in the Qimantage area, East Kunlun Orogen. *Geol. Rev.* **2026**, *72*, 33–49. (In Chinese with English abstract)
20. Geng, J.; Wang, Y.W.; Wang, X.Y.; Chen, Y. The chronology, origin, genesis and geodynamic background of Hercynian magmatic rocks in Niukutou area, Qinghai Province. *Chin. J. Geol.* **2025**, *60*, 165–190. (In Chinese with English abstract)
21. Wang, X.Y.; Zhu, X.Y.; Li, J.D.; Wang, Y.W.; Jiang, B.B.; Wu, J.R.; Huang, X.K.; Zhao, Z.Y. Two stage magmatisms and their skarn-type mineralization in the Niukutou ore district, Qinghai Province. *Acta Petrol. Sin.* **2021**, *37*, 1567–1586. (In Chinese with English abstract) [CrossRef]
22. Wang, X.Y.; Wang, S.L.; Wu, J.R.; Wang, H.; Zhu, X.Y.; Wang, Y.W.; Zhang, K.; Liu, M.; Yang, X.; Cai, Y.W. Mineralization age and ore forming–source of Niukutou Pb–Zn deposit, Qinghai: Evidence from geochronology of ore–forming rock bodies and Re–Os geochemistry of pyrite. *Northwest. Geol.* **2023**, *56*, 71–81. (In Chinese with English abstract)
23. Lu, H.F.; Chen, J.; Yu, F.C.; Xu, B.B.; Jiao, H. Study of genesis and geodynamic setting of diorite- porphyrite in Xiarihamu area: Constraints from geochronology, geochemistry and Hf isotopic data. *Mineral. Petrol.* **2019**, *39*, 61–68. (In Chinese with English abstract)
24. Guo, F.; Wang, P.X.; Bian, X.D.; Feng, N.Q. Geochronological and geochemical characteristics and geological significance of the monzogranite in Xiarihamu area of East Kunlun. *Geol. Surv. China* **2020**, *7*, 51–60. (In Chinese with English abstract)
25. Guo, F.; Wang, P.X.; Wang, Z.N.; Feng, N.Q. Geochemical and geochronology characteristics of retrograde eclogite in Xiarihamu area, East Kunlun Mountains, and its geological implications. *Sediment. Geol. Tethyan Geol.* **2020**, *40*, 45–55. (In Chinese with English abstract)
26. Wang, G.; Sun, F.Y.; Li, B.L.; Li, S.J.; Ao, C. Zircon U-Pb geochronology and geological significance of Early Devonian mafic dyke swarms in Xiarihamu ore district. *J. Heilongjiang Univ. Sci. Technol.* **2019**, *29*, 35–40. (In Chinese with English abstract)
27. Xiong, L.; Zhang, G.B.; Song, S.G.; Liu, S.Q.; Feng, D.; Chang, F. Eclogite in the East Kunlun Orogen, northwestern China: A record of the Neoproterozoic breakup of Rodinia and early Paleozoic continental subduction. *Geol. Soc. Am. Bull.* **2023**, *136*, 1413–1430. [CrossRef]
28. Yan, J.M.; Sun, F.Y.; Li, B.L.; Li, L.; Zhang, W.H.; Yan, Z.P.; Zhang, Y.S. Geochronological, geochemical, and mineralogical characteristics of the Akechukesai-I mafic–ultramafic complex in the eastern Kunlun area of the northern Tibet Plateau, west China: Insights into ore potential. *Ore Geol. Rev.* **2020**, *121*, 103468. [CrossRef]
29. Li, B.; Chen, J. Geochronology and geochemistry of an early Silurian plagiogranite from Xiarihamu area, East Kunlun, northwest China: Implications for Proto-Tethyan evolution. *Arab. J. Geosci.* **2021**, *14*, 794. [CrossRef]
30. Li, H.R.; Qian, Y.; Sun, F.Y.; Sun, J.L.; Wang, G. Zircon U–Pb dating and sulfide Re–Os isotopes of the Xiarihamu Cu–Ni sulfide deposit in Qinghai Province, Northwestern China. *Can. J. Earth Sci.* **2020**, *57*, 885–902. [CrossRef]
31. Feng, L.Q.; Shen, R.W.; Peng, Y.W.; Gu, X.X.; Zhang, Y.M.; Du, Z.L.; Wang, D.W. Genesis of Late Silurian to Early Devonian S-type granites in Kunlun River area, Qinghai Province and the tectonic evolution of the Proto-Tethys Ocean. *J. Chengdu Univ. Technol. (Sci. Technol. Ed.)* **2026**, *53*, 403–421. (In Chinese with English abstract)

32. Zhao, M.F.; Dong, J.E.; Qi, C.W.; Wei, Y.N.; Dong, X.J. The petrogenesis of the Early Devonian granites in the Tuolahaigou Area, Eastern Kunlun: Constraints from geochronology, geochemistry and Sr-Nd isotopes. *China Manganese Ind.* **2024**, *42*, 31–39. (In Chinese with English abstract)
33. Zhao, M.F.; Li, C.F.; Bao, S.D.; Dong, J.E.; Qi, C.W.; Shi, L.C.; Wei, Y.N.; Li, Y.L. Geochemical characteristics and tectonic significance of granites in the northern area of Dazaohuogou in East Kunlun. *J. Xian Univ. Sci. Technol.* **2024**, *44*, 748–758. (In Chinese with English abstract)
34. Wang, G.L.; Liu, J.D.; Yang, X.S.; Liu, R.; Cao, J.S.; Han, H.C.; Chen, L.J. Geochemistry, LA-ICP-MS zircon U-Pb ages of the Meicaogou ophiolite in East Kunlun, and its geological significance. *Geol. Bull. China* **2019**, *38*, 573–591. (In Chinese with English abstract)
35. Li, J.Q.; Wang, B.Z.; Wang, T.; Wang, M.; Li, Q.; Ma, Y.C. Genesis of Late Ordovician granite porphyry at Heicigou gold deposit, East Kunlun: Constraints from zircon U-Pb age, geochemistry and Sr-Nd-Pb-Hf isotopic systematics. *Geol. Bull. China* **2022**, *41*, 2173–2185. (In Chinese with English abstract) [CrossRef]
36. Yang, X.S.; Wang, G.L.; Yu, F.C.; Meng, H.; Zhao, J. Geochemical characteristics and geological significance of Late Ordovician granite in Yadongshan Area of Qinghai Province. *Min. Explor.* **2019**, *10*, 425–434. (In Chinese with English abstract)
37. Du, W.; Jiang, C.Y.; Xia, M.D.; Zhou, W.; Ling, J.L.; Wang, B.Y. A newly discovered Early Paleozoic ophiolite in Dagele, Eastern Kunlun, China, and its geological significance. *Geol. J.* **2017**, *52*, 425–435. [CrossRef]
38. Cao, J.S.; Xu, H.M.; Wang, J.; Wang, W.; Zheng, Y.; Ma, Y.C.; Hou, M.L.; Zhang, X.Y.; Li, Y.L.; Wang, T.; et al. Discovery of Late Silurian mafic-ultramafic intrusions and associated nickel-cobalt mineralization in the northern Dagelegou Area, East Kunlun. *Geotecton. Metallog.* **2026**, *50*, 451–475. (In Chinese with English abstract)
39. Wang, C.T.; Li, W.F.; Wang, B.Z.; Wang, Q.; Zhang, X.Y.; Wang, T.; Zheng, Y.; Jin, T.T.; Liu, J.D.; Yuan, B.W.; et al. Geochronology, geochemistry, Sr-Nd isotopic characteristics and geological significance of the pyroxenite in the Dagele alkali complex, East Kunlun. *Geotecton. Metallog.* **2024**, *48*, 125–147. (In Chinese with English abstract)
40. Li, Y.L.; Han, J.; Zhao, Z.Y.; Li, J.Q.; Wang, T.; Wang, B.Z.; Wang, T.S. Zircon U-Pb chronology, geochemistry, and geological significance of gabbros in southern Dagele farm, East Kunlun. *Geotecton. Metallog.* **2024**, *48*, 172–187. (In Chinese with English abstract)
41. Li, J.B.; Lü, Z.; Chen, Z.Y.; Liu, X.H. Metamorphic evolution of mafic two-pyroxene granulites in the Dagele area, East Kunlun. *Acta Petrol. Sin.* **2023**, *39*, 2636–2650. (In Chinese with English abstract) [CrossRef]
42. Wang, B.Z.; Wang, Q.; Wang, C.T.; Li, W.F.; Li, Y.L.; Jin, T.T.; Liu, J.D. Petrogenesis and geological significance of Devonian syenites in the Dagela area, East Kunlun. *Geotecton. Metallog.* **2024**, *48*, 61–86. (In Chinese with English abstract)
43. Zheng, Z.; Chen, Y.J.; Deng, X.H.; Yue, S.W.; Chen, H.J.; Wang, Q.F. Origin of the Bashierxi monzogranite, Qiman Tagh, East Kunlun Orogen, NW China: A magmatic response to the evolution of the Proto-Tethys Ocean. *Lithos* **2018**, *296–299*, 181–194. [CrossRef]
44. Zhang, H.H.; Li, X.L. Geochemical characteristics of the A-type granite in the Kaerqueka copper deposit in the East Kunlun orogenic belt, China: Implications for petrogenesis and tectonic setting. *Acta Mineral. Sin.* **2025**, *45*, 373–386. (In Chinese with English abstract) [CrossRef]
45. Wang, P.X.; Guo, F.; Wang, Z.N. Zircon U-Pb ages, geochemical features and geological implications of Middle Devonian granite in Wulanbaixing area, Qimantag area of East Kunlun Mountains. *Geol. Bull. China* **2020**, *39*, 194–205. (In Chinese with English abstract)
46. Ren, H.D.; Pan, T.; Wang, T.; Wang, B.Z.; Wang, X.X.; Zhang, J.J.; Wang, J.G.; Zhao, W.T. Geochronology and geochemistry of Paleozoic S-type granites in the western segment of the East Kunlun Orogen and its implications for tectonic evolution. *Acta Geol. Sin.* **2025**, *99*, 743–760. [CrossRef]
47. Zhao, C.T.; Chen, L.; Liu, Z.; Yu, D.M.; Ling, Z.Y.; Huo, S.L.; Han, J.J.; Li, P.; Li, Y.G.; Wang, J.P. The Genesis of Early Paleozoic Peraluminous Granite in the Heihai Region of East Kunlun Orogenic Belt and Its Constraints on Tectonic Evolution. *Acta Geosci. Sin.* **2026**, *47*, 118–134. (In Chinese with English abstract)
48. Lu, H.F.; Pan, T.; Jiao, H.; Ding, Q.F.; Zheng, T.; Zhou, X.; Wu, R.Z. Geochronology, geochemistry, and Hf isotopic compositions of the Early Devonian Heihaibei granite in the East Kunlun Orogen, Northwest China. *Can. J. Earth Sci.* **2022**, *59*, 566–579. [CrossRef]
49. Wang, Y.G.; He, X.Z.; Yu, D.L.; Han, H.Q.T.; Gao, K.; Gou, S.W.; Hua, W.Q.; Yang, S.C.; He, H.H. The genesis and geological significance of Early Devonian A2-type granite in Bairiqili area, western East Kunlun Mountains. *Geol. Rev.* **2024**, *70*, 1709–1726. (In Chinese with English abstract)
50. Sun, Y.M.; Li, B.L.; Li, P.; Li, C.X.; Li, Z.H.; Shi, Y.F. Geochronology, geochemistry, and Hf isotope of quartz monzonite and diorite in dachaigou, the East Kunlun orogenic belt, China, and their geological significance. *Can. J. Earth Sci.* **2024**, *61*, 760–776. [CrossRef]
51. Lei, Y.L.; Dai, J.W.; Bai, Q.; Wang, K.X.; Sun, L.Q.; Liu, X.D.; Yu, C.D.; He, S.W. Genesis and implications of peraluminous A-type rhyolite in the Haidewula area, East Kunlun Orogen. *Acta Petrol. Sin.* **2021**, *37*, 1964–1982. (In Chinese with English abstract) [CrossRef]

52. Han, Y.; Wang, Q.L.; Xie, H.L.; Chen, S.L.; Li, S.N.; Li, Y.L.; Wang, B.; Zhang, Z.Z.; Wang, L.; Ma, Z.Q.; et al. Geochemistry, zircon U-Pb chronology and Hf isotopes of the Baidungou granite from the East Kunlun Orogen and their implications. *Acta Petrol. Mineral.* **2024**, *43*, 1448–1464. (In Chinese with English abstract) [CrossRef]
53. Li, J.Y.; Qian, Y.; Li, H.R.; Sun, J.L.; Yang, X.M.; Chen, B.; Fan, X.Z.; Sun, F.Y. The Late Ordovician granitoids in the East Kunlun Orogenic Belt, Northwestern China: Petrogenesis and constraints for tectonic evolution of the Proto-Tethys Ocean. *Int. J. Earth Sci.* **2020**, *109*, 1439–1461.
54. Gao, Y.B.; Li, W.Y.; Qian, B.; Li, K.; Li, D.S.; He, S.Y.; Zhang, Z.W.; Zhang, J.W. Geochronology, geochemistry and Hf isotopic compositions of the granitic rocks related with iron mineralization in Yemaquan deposit, East Kunlun, NW China. *Acta Petrol. Sin.* **2014**, *30*, 1647–1665. (In Chinese with English abstract)
55. Bai, H.X.; Zhou, J.; Wang, J.Y.; Li, H.; Liu, B. Geological characteristics and prospecting prospects of East Niukutou deposit in Qimantage Area, East Kunlun. *Met. Mine* **2020**, 162–171. (In Chinese with English abstract)
56. Sun, F.Y.; Li, B.L.; Ding, Q.F.; Zhao, J.W.; Pan, T.; Yu, X.F.; Wang, L.; Chen, G.J.; Ding, Z.J. *Research on the Key Problems of Ore Prospecting in the Eastern Kunlun Metallogenic Belt*; Geological Survey Institute of Jilin University: Changchun, China, 2009. (In Chinese)
57. Wen, T.; Dong, J.L.; Wang, C.; Song, S.G. Two ophiolite belts in the East Kunlun Orogenic Belt record evolution from the Proto-Tethys to Paleo-Tethys Oceans. *Int. Geol. Rev.* **2023**, *65*, 1957–1976.
58. Rudnick, R. Making continental crust. *Nature* **1995**, *378*, 571–578. [CrossRef]
59. Li, W.; Yu, X.Q.; Hu, J.; Zhang, Y.C.; Peng, T.; Liu, N.W. Bidirectional subduction of the Proto-Tethys Ocean: Constraints from geochronology and geochemistry of S-type granites from Baoshan Block in western Yunnan (SW China). *J. Geol. Soc.* **2024**, *181*, jgs2022-188.
60. Zhang, Q.C.; Wu, Z.H.; Chen, X.H.; Zhou, Q.; Shen, N.S. Proto-Tethys oceanic slab break-off: Insights from early Paleozoic magmatic diversity in the West Kunlun Orogen, NW Tibetan Plateau. *Lithos* **2019**, *346–347*, 105147. [CrossRef]
61. Zeng, R.Y.; Wang, Q.F.; Santosh, M.; Allen, M.B.; Su, H.; Ju, P.J.; Yuan, Z.Q.; Zhang, Y.; Zhang, X.X.; Liu, G.X. Early Paleozoic Tethyan evolution and metallogeny in East Asia. *Ore Geol. Rev.* **2025**, *186*, 106890. [CrossRef]
62. Sláma, J.; Košler, J.; Condon, D.J.; Crowley, J.L.; Gerdes, A.; Hanchar, J.M.; Horstwood, M.S.A.; Morris, G.A.; Nasdala, L.; Norberg, N.; et al. Plešovice zircon—A new natural reference material for U-Pb and Hf isotopic microanalysis. *Chem. Geol.* **2008**, *249*, 1–35. [CrossRef]
63. Wiedenbeck, M.; Alle, P.; Corfu, F.; Griffin, W.L.; Meier, M.; Oberli, F.; von Quadt, A.; Roddick, J.C.; Spiegel, W. Three natural zircon standards for U-Th-Pb, Lu-Hf, trace element and REE analyses. *Geostand. Newsl.* **1995**, *19*, 1–23. [CrossRef]
64. Liu, Y.S.; Gao, S.; Hu, Z.C.; Gao, C.G.; Zong, K.Q.; Wang, D.B. Continental and oceanic crust recycling-induced melt-peridotite interactions in the Trans-North China Orogen: U-Pb dating, Hf isotopes and trace elements in zircons from mantle xenolths. *J. Petrol.* **2010**, *51*, 537–571.
65. Andersen, T. Correction of Common Lead in U-Pb Analyses That do not Report ^{204}Pb. *Chem. Geol.* **2002**, *192*, 59–79. [CrossRef]
66. Ludwig, K.R. *User's Manual for Isoplot Version 3.75–4.15: A Geochronological Toolkit for Microsoft Excel*; Berkeley Geochronological Center Special Publication: Berkeley, CA, USA, 2012; Volume 5.
67. Middlemost, E.A.K. Naming materials in the magma/igneous rock system. *Earth-Sci. Rev.* **1994**, *37*, 215–224. [CrossRef]
68. Irvine, T.N.; Baragar, W.R.A. A guide to the chemical classification of the common volcanic rocks. *Can. J. Earth Sci.* **1971**, *8*, 523–548. [CrossRef]
69. Peccerillo, A.; Taylor, S.R. Geochemistry of eocene calc–alkaline volcanic rocks from the Kastamonu area, Northern Turkey. *Contrib. Mineral. Petrol.* **1976**, *58*, 63–81. [CrossRef]
70. Maniar, P.D.; Piccoli, P.M. Tectonic discrimination of granitoids. *Geol. Soc. Am. Bull.* **1989**, *101*, 635–643. [CrossRef]
71. Sun, S.S.; McDonough, W.F. Chemical and isotopic systematics of oceanic basalts: Implications for mantle composition and processes. *Geol. Soc. Spec. Publ.* **1989**, *42*, 313–345. [CrossRef]
72. Chappell, B.W.; White, A.J.R. Two contrasting granite types. *Pac. Geol.* **1974**, *8*, 173–174.
73. Loiselle, M.C.; Wones, D.R. Characteristics and origin of anorogenic granites. *Geol. Soc. Am.* **1979**, *11*, 468.
74. Eby, G.N. Chemical subdivision of the A-type granitoids: Petrogenetic and tectonic implications. *Geology* **1992**, *20*, 641–644. [CrossRef]
75. Hine, R.; Williams, I.S.; Chappell, B.W.; White, A.J.R. Contrasts between I- and S-type granitoids of the Kosciusko Batholith. *J. Geol. Soc. Aust.* **1978**, *25*, 219–234. [CrossRef]
76. King, P.L.; Chappell, B.W.; Allen, C.M.; White, A.J.R. Are A-type granites the high-temperature felsic granites? Evidence from fractionated granites of the Wangrah Suite. *Aust. J. Earth Sci.* **2001**, *48*, 501–514. [CrossRef]
77. Yang, J.H.; Wu, F.Y.; Chung, S.L.; Wilde, S.A.; Chu, M.F. A hybrid origin for the Qianshan A-type granite, northeast China: Geochemical and Sr-Nd-Hf isotopic evidence. *Lithos* **2006**, *89*, 89–106. [CrossRef]
78. Whalen, J.B.; Currie, K.L.; Chappell, B.W. A-type granites: Geochemical characteristics, discrimination and petrogenesis. *Contrib. Mineral. Petrol.* **1987**, *95*, 407–419. [CrossRef]

79. Wu, F.Y.; Sun, D.Y.; Li, H.M.; Jahn, B.M.; Wilde, S. A-type granites in Northeastern China: Age and geochemical constraints on their petrogenesis. *Chem. Geol.* **2002**, *187*, 143–173. [CrossRef]
80. Zen, E.A. Aluminum enrichment in silicate melts by fractional crystallization: Some mineralogic and petrographic constraints. *J. Petrol.* **1986**, *27*, 1095–1117. [CrossRef]
81. Chappell, B.W. Aluminium saturation in I-and S-type granites and the characterization of fractionated haplogranites. *Lithos* **1999**, *46*, 535–551. [CrossRef]
82. Chappell, B.W.; Stephens, W.E. Origin of infracrustal (I-type) granite magmas. *Earth Environ. Sci. Trans. R. Soc. Edinb.* **1988**, *79*, 71–86. [CrossRef]
83. Richards, J.P. Magmatic to hydrothermal metal fluxes in convergent and collided margins. *Ore Geol. Rev.* **2011**, *40*, 1–26. [CrossRef]
84. Wu, F.Y.; Jahn, B.M.; Wilde, S.A.; Lo, C.H.; Yui, T.F.; Lin, Q.; Ge, W.C.; Sun, D.Y. Highly fractionated I-type granites in NE China (I): Geochronology and petrogenesis. *Lithos* **2003**, *66*, 241–273. [CrossRef]
85. Wu, F.Y.; Jahn, B.M.; Wilde, S.A.; Lo, C.H.; Yui, T.F.; Lin, Q.; Ge, W.C.; Sun, D.Y. Highly fractionated I-type granites in NE China (II): Isotopic geochemistry and implications for crustal growth in the Phanerozoic. *Lithos* **2003**, *67*, 191–204. [CrossRef]
86. Wang, X.S.; Bi, X.W.; Leng, C.B.; Zhong, H.; Tang, H.F.; Chen, Y.W.; Yin, G.H.; Huang, D.Z.; Zhou, M.F. Geochronology and geochemistry of Late Cretaceous igneous intrusions and Mo–Cu–(W) mineralization in the southern Yidun Arc, SW China: Implications for metallogenesis and geodynamic setting. *Ore Geol. Rev.* **2014**, *61*, 73–95. [CrossRef]
87. Champion, D.C.; Chappell, B.W. Petrogenesis of felsic I-type granites: An example from northern Queensland. *Earth Environ. Sci. Trans. R. Soc. Edinb.* **1992**, *83*, 115–126. [CrossRef]
88. Patiño Douce, A.E. Generation of metaluminous A-type granites by low-pressure melting of calc-alkaline granitoids. *Geology* **1997**, *25*, 743–746. [CrossRef]
89. Skjerlie, K.P.; Johnston, A.D. Fluid-absent melting behavior of an F-rich tonalitic gneiss at mid-crustal pressures: Implications for the generation of anorogenic granites. *J. Petrol.* **1993**, *34*, 785–815. [CrossRef]
90. Mazzucchelli, M.; Rivalenti, G.; Vannucci, R.; Bottazzi, P.; Ottolini, L.; Hofmann, A.W.; Parenti, M. Primary positive Eu anomaly in clinopyroxenes of low-crust gabbroic rocks. *Geochim. Cosmochim. Acta* **1992**, *56*, 2363−2370. [CrossRef]
91. Rudnick, R.; Gao, S. The role of lower crustal recycling in continent formation. *Geochim. Cosmochim. Acta Suppl.* **2003**, *67*, 403.
92. Weaver, B.L. The origin of ocean island basalt end-member compositions: Trace element and isotopic constraints. *Earth Planet. Sci. Lett.* **1991**, *104*, 381–397. [CrossRef]
93. Zhang, Q.; Wang, Y.L.; Jin, W.J.; Jia, X.Q.; Li, C.D. Criteria for the recognition of pre-, syn- and post- orogenic granitic rocks. *Geol. Bull. China* **2008**, *27*, 1–18. (In Chinese with English abstract)
94. Pearce, J.A. Sources and Settings of Granitic Rocks. *Episodes* **1996**, *19*, 120–125. [CrossRef]
95. Pearce, J.A.; Harris, N.B.W.; Tindle, A.G. Trace element discrimination diagrams for the tectonic interpretation of granitic rocks. *J. Petrol.* **1984**, *25*, 956–983. [CrossRef]
96. Hu, C.B.; Li, M.; Feng, C.Y.; Zha, X.F.; Gao, X.F.; Meng, J. Petrogenesis and metallogenic potential of the early devonian Yugusayi mafic-ultramafic complex in Qimantagh, East Kunlun orogeic belt. *Int. Geol. Rev.* **2023**, *65*, 1056–1076.
97. Dong, Y.P.; Sun, S.S.; He, D.F.; Hui, B.; Qi, N.; Sun, J.P.; Zhou, B.; Zang, R.T.; Zhang, B.; Liu, X.M. Early Paleozoic back-arc basin in the East Kunlun Orogen, northern Tibetan Plateau: Insight from the Wutumeiren ophiolitic mélange. *Lithos* **2024**, *464–465*, 107460. [CrossRef]
98. Dong, J.L.; Song, S.G.; Su, L.; Allen, M.B.; Li, Y.G.; Wang, C. Early Devonian mafic igneous rocks in the East Kunlun Orogen, NW China: Implications for the transition from the Proto- to Paleo-Tethys oceans. *Lithos* **2020**, *376–377*, 105771. [CrossRef]
99. Wang, H.; Feng, C.; Li, R.; Li, D. Geological characteristics, metallogenesis, and tectonic setting of porphyry–skarn Cu deposits in East Kunlun Orogen. *Geol. J.* **2018**, *53*, 58–76. [CrossRef]
100. Zhang, R.L.; Yuan, F.; Deng, Y.F.; Xu, H.Q.; Zhou, T.F.; Wang, F.Y.; Wang, Z.Q.; Li, Y.; Han, J.J.; Zhang, F.F. Implications of garnet composition on metallogenic chronology and ore-forming fluid evolution of skarn deposits: A case study of the Kendekeke Fe-polymetallic deposit in East Kunlun. *Ore Geol. Rev.* **2024**, *168*, 106020. [CrossRef]
101. Zhong, S.H.; Feng, C.Y.; Seltmann, R.; Li, D.X. Middle Devonian volcanic rocks in the Weibao Cu–Pb–Zn deposit, East Kunlun Mountains, NW China: Zircon chronology and tectonic implications. *Ore Geol. Rev.* **2017**, *84*, 309–327. [CrossRef]
102. Zou, Y.H.; Liu, Y.; Dai, T.G.; Mao, X.C.; Lei, Y.B.; Lai, J.Q.; Tian, H.L. Finite difference modeling of metallogenic processes in the Hutouya Pb-Zn deposit, Qinghai, China: Implications for hydrothermal mineralization. *Ore Geol. Rev.* **2017**, *91*, 463–476. [CrossRef]
103. Yin, S.; Ma, C.Q.; Xu, J.N. Geochronology, geochemical and Sr-Nd-Hf-Pb isotopic compositions of the granitoids in the Yemaquan orefield, East Kunlun orogenic belt, northern Qinghai-Tibet Plateau: Implications for magmatic fractional crystallization and sub−solidus hydrothermal alteration. *Lithos* **2017**, *294−295*, 339−355.
104. Chen, J.; Wang, B.Z.; Li, B.; Zhang, Z.Q.; Qiao, B.X.; Jin, T.T. Zircon U–Pb ages, geochemistry, and Sr–Nd–Pb isotopic compositions of Middle Triassic granodiorites from the Kaimuqi area, East Kunlun, Northwest China: Implications for slab breakoff. *Int. Geol. Rev.* **2015**, *57*, 257–270. [CrossRef]

105. Yao, L.; Lü, Z.C.; Zhao, C.S.; Pang, Z.S.; Yu, Z.S.; Yang, T.; Li, Y.S.; Liu, P.; Zhang, M.C. Zircon U–Pb geochronological, trace element, and Hf isotopic constraints on the genesis of the Fe and Cu skarn deposits in the Qiman Tagh area, Qinghai Province, Eastern Kunlun Orogen, China. *Ore Geol. Rev.* **2017**, *91*, 387–403. [CrossRef]
106. Zhong, S.H.; Li, S.Z.; Feng, C.Y.; Liu, Y.J.; Santosh, M.; He, S.Y.; Qu, H.Y.; Liu, G.Y.; Seltmann, R.; Lai, Z.Q.; et al. Porphyry copper and skarn fertility of the northern Qinghai-Tibet Plateau collisional granitoids. *Earth-Sci. Rev.* **2021**, *214*, 103524. [CrossRef]
107. Atherton, M.P.; Ghani, A.A. Slab breakoff: A model for Caledonian, Late Granite syn−collisional magmatism in the orthotectonic (metamorphic) zone of Scotland and Donegal, Ireland. *Lithos* **2002**, *62*, 65−85. [CrossRef]
108. Zhang, J.Y.; Ma, C.Q.; Xiong, F.H.; Liu, B.; Li, J.W.; Pan, Y.M. Early Paleozoic high-Mg diorite-granodiorite in the eastern Kunlun Orogen, western China: Response to continental collision and slab break-off. *Lithos* **2014**, *210−211*, 129−146.
109. Ding, Q.F.; Song, K.; Zhang, Q.; Yan, W.; Liu, F. Zircon U-Pb geochronology and Hf isotopic constraints on the petrogenesis of the Late Silurian Shidonggou granite from the Wulonggou area in the Eastern Kunlun Orogen, Northwest China. *Int. Geol. Rev.* **2019**, *61*, 1666−1689.
110. Zhang, J.Y.; Ma, C.Q.; Li, J.W.; Pan, Y.M. A possible genetic relationship between orogenic gold mineralization and post-collisional magmatism in the eastern Kunlun Orogen, western China. *Ore Geol. Rev.* **2017**, *81*, 342−357. [CrossRef]
111. Zhang, J.Y.; Lei, H.L.; Ma, C.Q.; Li, J.W.; Pan, Y.M. Silurian-Devonian granites and associated intermediate-mafic rocks along the eastern Kunlun Orogen, western China: Evidence for a prolonged post-collisional lithospheric extension. *Gondwana Res.* **2021**, *89*, 131−146. [CrossRef]
112. Zhong, S.H.; Huang, Y.; Liu, Y.L.; Zhang, Y.; Bai, G.L.; Liu, Z.G.; Ma, Q.; Wang, L.J.; Zhao, F.R.; He, S.Y. Silurian-Devonian critical metal mineralization boom of the East Kunlun Orogenic Belt. *Geol. Bull. China* **2025**, *44*, 574−586. (In Chinese with English abstract)
113. Li, X.H.; Liang, G.Z.; Wu, J.J.; Yang, K.F.; Fan, H.R.; Zeng, Q.D.; Zhang, Z.M.; Hu, F.F. Two periods of gold mineralization-magmatism-tectonism in the East Kunlun metallogenic belt. *Acta Petrol. Sin.* **2025**, *41*, 526−543. (In Chinese with English abstract) [CrossRef]
114. Sato, K. Sedimentary crust and metallogeny of granitoid affinity: Implications from the geotectonic histories of the circum-Japan Sea region, central Andes and southeastern Australia. *Resour. Geol.* **2012**, *62*, 329−351. [CrossRef]
115. Park, J.W.; Campbell, I.H.; Kim, J.; Moon, J.W. The role of late sulfide saturation in the formation of a Cu-and Au-rich magma: Insights from the platinum group element geochemistry of NiuatahiMotutahi lavas, Tonga rear arc. *J. Petrol.* **2015**, *56*, 59−81. [CrossRef]
116. Deng, Z.; Zhong, S.H.; Yan, J.Y.; Seltmann, R.; Dolgopolova, A.; Tang, H.J.; He, S.Y.; Luo, C.H. Magma mixing formed mineralized Middle–Late Triassic granitoids in the Qimantagh Metallogenic Belt, NW China: A case study from the Hutouya skarn deposit. *Ore Geol. Rev.* **2024**, *171*, 106192. [CrossRef]
117. Fan, J.J.; Wang, Q.; Li, J.; Wei, G.J.; Wyman, D.; Zhao, Z.H.; Liu, Y.; Ma, J.L.; Zhang, L.; Wang, Z.L. Molybdenum and boron isotopiccompositions of porphyry Cu mineralization-related adakitic rocks in Central-Eastern China: New insights into their petrogenesis and crust-mantle interaction. *J. Geophys. Res. Solid Earth* **2020**, *125*, e2020JB020474. [CrossRef]
118. Zhou, J.; Jin, C.; Suo, Y.H.; Li, S.Z.; Zhang, L.; Liu, Y.M.; Wang, G.Z.; Wang, P.C.; Dai, L.M.; Santosh, M. The Yanshanian (Mesozoic) metallogenesis in China linked to crust-mantle interaction in the western Pacific margin: An overview from the Zhejiang Province. *Gondwana Res.* **2022**, *102*, 95−132. [CrossRef]
119. Yang, L.Q.; Deng, J.; Zhang, L.; Zhao, A.H.; Santosh, M.; Yu, X.F.; Yang, W.; Li, D.P.; Shan, W.; Xie, D.; et al. Mantle-rooted fluid pathways and world-class gold mineralization in the giant Jiaodong gold province: Insights from integrated deep seismic reflection and tectonics. *Earth-Sci. Rev.* **2024**, *255*, 104862. [CrossRef]

Disclaimer/Publisher's Note: The statements, opinions and data contained in all publications are solely those of the individual author(s) and contributor(s) and not of MDPI and/or the editor(s). MDPI and/or the editor(s) disclaim responsibility for any injury to people or property resulting from any ideas, methods, instructions or products referred to in the content.